Inorganic Chemistry

ARTICLE

pubs.acs.org/IC

# Iron(II) Vacataporphyrins: A Variable Annulene Conformation inside a Regular Porphyrin Frame

Ewa Pacholska-Dudziak,* Aneta Gaworek, and Lechosław Latos-Grażyński*

Department of Chemistry, University of Wrocław, ul. F. Joliot-Curie 14, 50-383 Wrocław, Poland

Supporting Information

**ABSTRACT:** 5,10,15,20-Tetraaryl-21-vacataporphyrin (**1**), an annulene−porphyrin hybrid containing a butadiene fragment in the macrocycle perimeter, gives paramagnetic iron(II) complexes **2**. The porphyrin **1** is devoid of one donor atom of the coordination core; hence, metal ion is bound in the macrocyclic cavity by only three pyrrolic nitrogen atoms. The coordination sphere in **2-X** (where X = Cl, Br, I) is completed by a halide anion. The butadiene fragment flexibility and constraints of coordination lead to two stereoisomers with the chain oriented inward (**2-i-X**) or outward (**2-o-X**) of the macrocyclic center. Axial halide subtraction ($AgBF_4$ addition) leads to two new forms differing in the butadiene chain configuration. The $^1$H NMR spectra of all complexes show characteristics typical for high-spin iron(II) complexes of porphyrinoids. The dependence of the relaxation times $T_1$ versus $Fe^{II}\cdots H$ distances (estimated by MM+ models) for three of the isomers is in accordance with the **in**, **out**, and/or **zigzag** geometries. The **2-o-X** complex is more reactive than **2-i-X** and reacts at room temperature with dioxygen to form the iron(II) 21-oxaporphyrin complex, conserving the iron(II) oxidation state. After the addition of imidazole or excess of methanol to a mixture of **2-o-X** and **2-i-X**, single five-coordinate complexes with **out** annulene configuration and two axial ligands are formed.

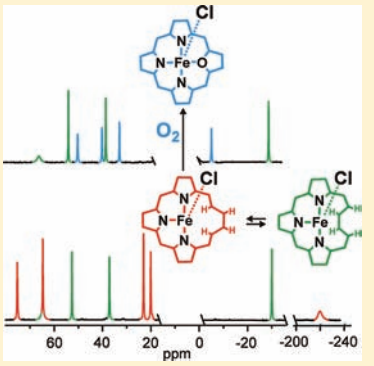


## INTRODUCTION

The chemistry of iron porphyrins has been strongly stimulated by the need to understand the functions and catalytic processes of various biologically important heme proteins. Iron porphyrins as functional and spectroscopic models of the active sites of hemoglobins, peroxidases, cytochromes, etc., have been synthesized and widely studied by a number of techniques. Among them, the nuclear magnetic resonance (NMR) of paramagnetic molecules is particularly useful because it provides detailed information on the electronic structure of the complexes in a solution or in a protein pocket.[1−3] The iron(III) and high-spin iron(II) d orbitals with unpaired electron(s) interact with specific molecular orbitals of a porphyrin and increase the spin density at specific carbon and nitrogen atoms of the complex. Consequently, the NMR signals of the attached protons exhibit paramagnetic shifts arranging in specific spectral patterns dependent on the iron ion configuration.[4−10] The electronic structure of iron porphyrins is controlled by the number and field strength of axial ligands and by the macrocycle deformations.[11,12] The porphyrin distortions from planarity are commonly observed in naturally occurring heme proteins because the deformations are induced by the protein environment.[13−15] Thus, changes in the nonplanarity may provide a mechanism for protein modulation of the biological properties. It is suggested that the flexibility of the porphyrin ring is important in some biocatalytic processes, for example, involved as a key transition-state intermediate of the active site of ferrochelatase.[14−16]

Nonplanar porphyrin conformations are accomplished by the introduction of sterically demanding residues in the porphyrin core or at the periphery (alkylation and arylation), as well as the coordination of metal ions of maladjusted size.[17] Core-modified porphyrins, formed by the replacement of one or more nitrogen atoms by other heteroatom(s), i.e., heteroporphyrins sometimes demonstrate nonplanar arrangements, but generally the distortions are much more distinct in the metalated macrocycles (for example, thiaporphyrin complexes).[18−20] A special chapter is constituted by carbaporphyrin metal complexes, where a hydrocarbon moiety does not form a $\sigma$ bond with a metal but remains in a strongly tilted position with a side-on coordination or weak interaction.[21] Widely studied benziporphyrin and inverted porphyrin complexes provide good illustrations.[22,23] Searching for borders of porphyrin flexibility leads to a unique core-modified porphyrin, with a severely distorted basic porphyrin framework, i.e., ditelluraporphyrin

**Chart 1. 5,10,15,20-Tetraphenyl-21,23-ditelluraporphyrin**

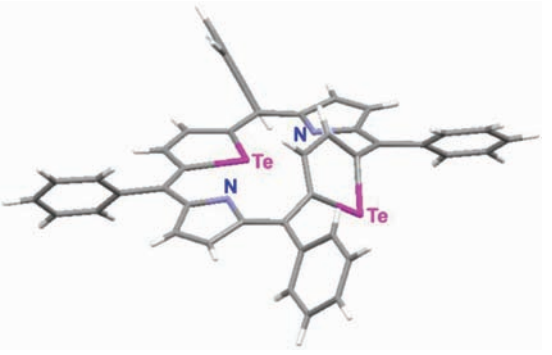


**Received:** July 18, 2011
**Published:** September 27, 2011

  

**Chart 2. 5,10,15,20-Tetraaryl-21-vacata- and 21,23-divacataporphyrins**

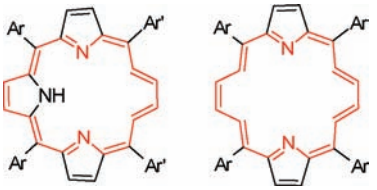


(Chart 1), with one tellurophene moiety rotated and pointing with the tellurium atom outward.[24] This sort of tilt and possible rotation was discovered also in *p*-benziporphyrin and naphthiporphyrin.[25−27]

A significant skeleton flexibility was also reached by a different sort of core modifications: subtraction of successive nitrogen atoms of the porphyrin core. According to the commonly accepted [18]annulene model of porphyrin aromaticity, the two NH moieties may be treated as bridging linkers of diaza[18]annulene, making the porphyrin macrocycle rigid, contrary to a nonbridged [18]annulene. Hybrid annulene−porphyrin molecules were synthesized, i.e., partially bridged diazaannulenes, preserving their aromaticity and a porphyrin-like skeleton in general, however showing much larger flexibility than regular porphyrins. Two steps of bridge removal have led to 21-vacataporphyrin[28] and 21,23-divacataporphyrin (dideazaporphyrin)[29,30] (Chart 2). The first molecule shows elasticity only after metal ion insertion, but for the second macrocycle, its flexibility results in the existence of another, minor conformer, different from the main form in the configuration of the two (bridge-devoid) annulene moieties.[30]

21-Vacataporphyrin reveals a unique structural flexibility triggered by the coordination of cadmium(II), zinc(II), nickel(II), and particularly palladium(II).[31−33] The structural rearrangements of the annulene fragment lead to two general modes of interaction between the palladium ion and annulene moiety: $\sigma$ coordination through a deprotonated, trigonally hybridized carbon atom (C2) of the butadiene segment and $\eta^2$-type interaction involving the C2−C3 unit of the butadiene part. The coordinated vacataporphyrin acquires Hückel or extremely rare Möbius topologies, readily reflected by the spectroscopic properties. Palladium vacataporphyrin complexes reveal Hückel aromaticity or Möbius antiaromaticity of a [18]annulene 18$\pi$-electron circuit, applying the butadiene fragment as a topology selector.[32]

Here we introduce vacataporphyrin as a ligand for iron(II) and study the system by means of $^1$H NMR, profitting from the paramagnetic properties of the complexes to gain a complementary characterization of the isomerism. The deazaporphyrin ligand is probed by iron(II) as a paramagnetic sensor, and the influence of one nitrogen absence on the spin delocalization is examined. Thus, we report the synthesis of iron(II) vacataporphyrin complexes and their isomerism and unusual reactivity toward dioxygen.

## RESULTS AND DISCUSSION

**Synthesis.** 5,20-Diphenyl-10,15-bis(4-methoxyphenyl)-21-vacataporphyrin (**1**)[28] reacts readily with iron(II) chloride or bromide in boiling tetrahydrofuran (THF) to give paramagnetic high-spin iron(II) vacataporphyrin complexes **2-Cl** or **2-Br**, respectively. The absence of oxygen is crucial for the reaction accomplishment (for the product purity). The macrocyclic ligand is monoanionic, and one halide ligand is required to form a neutral complex. If iron pentacarbonyl and iodine are used instead of a metal salt, the reaction yields a similar complex, **2-I**, with axially bound iodide (Scheme 1). The products are stable in oxygen-free solutions.

**Scheme 1. Synthesis of the Iron Vacataporphyrin Complexes**

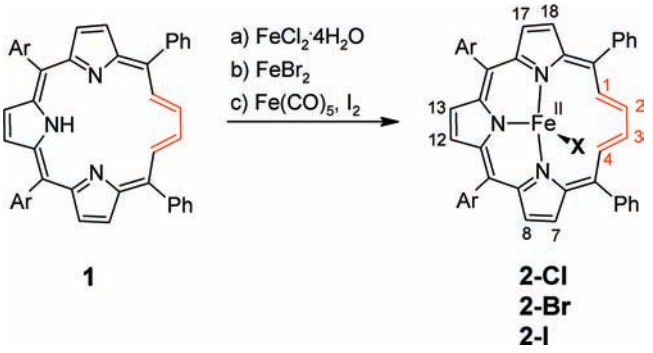


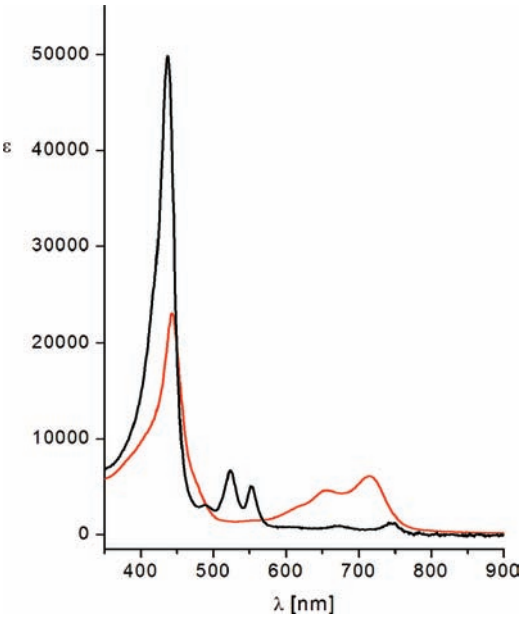


**Figure 1.** UV−vis spectra of **1** (black line) and **2-Br** (red line) in toluene.

The porphyrinoid ligand with three nitrogen donors, if shaped as presented in Scheme 1, is tridendate. Still, there is a fourth equatorial site: the "vacated 21-position" within the porphyrin plane, fenced by the annulene moiety. A bond formation between the central ion and the C1−C2−C3−C4 chain would require configuration changes, which were observed in already published vacataporphyrin complexes.[31,32] The halide ligand makes, therefore, the firm fourth donor. In fact, this ligand is not expected to occupy the axial position of the square-pyramid structure but, in analogy to known vacataporphyrin complexes, may be rather directed toward the annulene side, affording the coordinating environment of iron(II).

The electronic absorption spectrum of **2-Br** is shown in Figure 1, together with the spectrum of the free ligand **1**. A metalloporphyrin-like pattern is clearly present with a distinct Soret-like band (443 nm) and a set of bands in the Q region. The spectral pattern resembles that of analogous cadmium, zinc, and palladium complexes.[31,32]

**$^1$H NMR of 2.** The $^1$H NMR spectrum of a representative spectrum of the iron vacataporphyrin complex **2-Cl** in toluene-$d_8$ is shown in Figure 2. The selected spectral parameters of all three complexes **2-X** (X = Cl, Br, I) are gathered in Table 1. The spectra show characteristics typical for high-spin iron(II) porphyrins and,


dx.doi.org/10.1021/ic2015176 |*Inorg. Chem.* 2011, 50, 10956–10965

more closely, core-modified porphyrin analogues. Each spectrum displays nine paramagnetically shifted signals outside the diamagnetic region, which largely fall in the region from +75 to −30 ppm, but one peak is distinctly shifted up to −163 to −220 ppm (depending on the axial halide). Taking into consideration the symmetry of the vacataporphyrin ligand and the predicted 2-fold symmetry of the formed complex ($C_s$), we expect only five strongly shifted signals for **2**: three pyrrole and two annulene resonances. A careful integration indicates that the signals are differentiated by their intensities into two sets, assigned to two isomeric forms of **2**. Similar isomers were detected for diamagnetic vacataporphyrin complexes with cadmium(II) and zinc(II) and for paramagnetic complexes with nickel(II).[31] The first set of five signals, marked in red, is assigned (in the $T_1$ experiment, see below) to a form denoted as **2-o** with a typical porphyrin-like perimeter, i.e., with an **out** configuration of the butadiene (annulene) fragment (Scheme 2). All of the $\beta$-pyrrolic and 2,3-butadiene protons are shifted downfield. On the low frequency side of the spectrum, a single strongly shifted broad signal is present [−163 (**2-I**) to −220 ppm (**2-Cl**) in 298 K], assigned to the inner 1,4-H protons. The second set of signals (green) comes from form **2-i**, with the butadiene fragment strongly bent **in**. For this form, four signals with large paramagnetic shifts were readily detected. The missing fifth signal of 1,4-H was eventually identified in the inversion−recovery experiment in the diamagnetic region (−0.93 ppm for **2-i-Cl**) and, independently, in the $^2$H NMR spectrum of specifically deuterated **2-Br**-$d_x$ and **2-I**-$d_x$ complexes (Table 1).

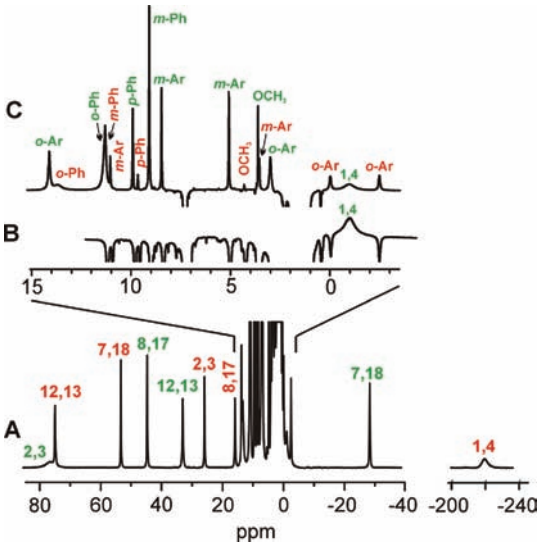


**Figure 2.** $^1$H NMR spectra (300 K, 600 MHz, toluene-$d_8$) of (A) **2-Cl** (isomer **out** marked in red and isomer **in** in green) (B and C) the diamagnetic region. Spectra were acquired by an inversion−recovery technique, with delay times $\tau$ = 2 ms for part B and $\tau$ = 100 ms for part C; Ar denotes the 4-methoxyphenyl group.

**Signal Assignment: Deuteration and $T_1$ Studies.** The assignment of signals for each form of **2-X** was done on the basis of a detailed $^1$H NMR signal intensity comparison of specifically deuterated compounds and $T_1$ relaxation time analysis. 2D NOESY and COSY experiments were helpful in a few favorable cases only. The deuterated ligand **1**-$d_x$ was synthesized as published before,[31] and the degree of deuteration (**x**) varied much depending on the reaction conditions. In every case, deuteration was attained not only at the 1 and 4 positions of deuterium substitution as expected but also at the $\beta$-pyrrole positions as well and in a very diverse level (14−77%) at the 2,3-carbon atoms of the butadiene chain. Eventually, the degree of deuteration for each position was precisely determined for each sample by integration of the $^1$H NMR signals of a free ligand and was the basis for $\beta$-pyrrole and butadiene signal assignment.

**Scheme 2. Conformational Rearrangement of Two Isomers of Complexes 2-X (X = Cl, Br, I)**

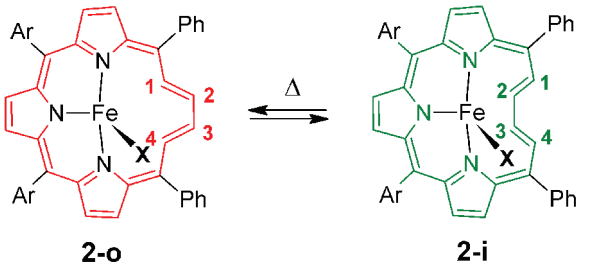


**Table 1. $^1$H NMR Chemical Shifts for 2-Cl, 2-Br, and 2-I, Including *meso*-Aryl Signals for 2-Cl (Data in Toluene-$d_8$ Solutions, at 300 K, Except for Footnotes a and b)**

| | isomer **2-o** | | | | | isomer **2-i** | | | | |
|---|---|---|---|---|---|---|---|---|---|---|
| | butadiene | | pyrroles | | | butadiene | | pyrroles | | |
| | 1,4-H | 2,3-H | 12,13-H | 7,18-H | 8,17-H | 1,4-H | 2,3-H | 12,13-H | 7,18-H | 8,17-H |
| **2-Cl** | −220.05 | 25.98 | 75.19 | 53.47 | 15.26 | −0.93 | 76.15 | 33.07 | −28.33 | 44.64 |
| **2-Br** | −195.29 | 24.79 | 75.74 | 58.89 | 17.33 | 3.90[a] | 71.33 | 35.05 | −29.86 | 47.38 |
| **2-I** | −163.13 | 23.26 | 75.61 | 65.11 | 20.15 | 3.83[b] | 65.11 | 37.40 | −31.06 | 52.93 |

| | aryl **2-o-Cl** | | | | aryl **2-i-Cl** | | | |
|---|---|---|---|---|---|---|---|---|
| | ortho | meta | para | $OCH_3$ | ortho | meta | para | $OCH_3$ |
| phenyl | 13.32 | 10.94 | 9.35 | | 11.03 | 8.82 | 9.62 | |
| 4-methoxy-phenyl | −0.24 | 10.70 | | 4.07 | 13.76 | 8.20 | | 3.41 |
| | −2.53 | 3.38 | | | 2.81 | 4.87 | | |

[a] Detected in 1,4-deuterated **2-Br** in 300 K (benzene) in a $^2$H NMR experiment. [b] Detected in 1,4-deuterated **2-I** in 350 K (toluene) in a $^2$H NMR experiment.


dx.doi.org/10.1021/ic2015176 |*Inorg. Chem.* 2011, 50, 10956–10965

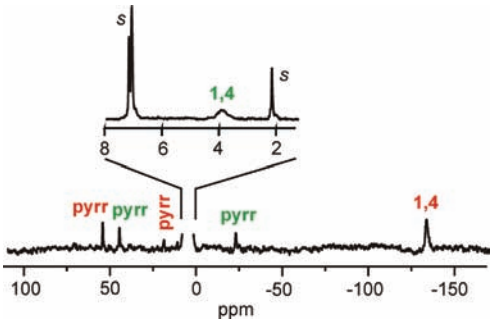


**Figure 3.** $^2$H NMR spectrum (77 MHz, toluene, 350 K) of **2-I**. Partially deuterated pyrrole positions (7, 8, 17, and 18) give signals of smaller intensity.

The $^2$H NMR spectrum (Figure 3) measured for the deuterated complex **2-I**$d_x$ allowed for the unambiguous identification of 1,4-H signals, particularly eluding for the **in** form. $^1$H NMR of **2-I**$d_x$ measured at different temperatures allowed assignment of the porphyrin perimeter signals.

The assignment of two sets of signals to respective structures **2-o-Cl** and **2-i-Cl** was done on the basis of the relaxation times. For **2-Br** and **2-I**, the assignments followed those for **2-Cl**. We considered the significant line broadening of resonances of annulene protons, 1,4-H and 2,3-H, expressing short $T_2$ ($T_2$*) relaxation times, caused by the proximity of the paramagnetic iron(II) center. The $^1$H NMR pattern with one such broad signal was assigned to the geometry of **2-o-X** with 1,4-H pointing toward iron(II), whereas the second set of resonances with two broad peaks was attributed to **2-i-X**, where both 1,4-H and 2,3-H of a strongly bent butadiene moiety are expected to relax rapidly.

For semiquantitative analysis, $T_1$ relaxation times were chosen because they are independent of exchange effects, contrary to $T_2$. Assuming that dipolar relaxation dominates over contact relaxation, as is the common situation for iron porphyrins, the inverse of relaxation times $T_1$ is proportional to $\tau_c/r^6$, where $\tau_c$ is the rotational correlation time of a molecule and $r$ is the distance between the (relaxing) nucleus (here a proton) and a paramagnetic metal center [iron(II)]. Simply

$$T_1 \sim r^6$$

where the proportionality constant is equal for all of the protons of one molecule. The $T_1$ relaxation times were measured for **2-Cl** by the inversion−recovery experiments in toluene-$d_8$ at three different temperatures. The data for 298 K are gathered in Table 2.

The values fall into distinct ranges: (1) below 1 ms for the crucial 1,4-H of both forms and 2,3-H for **2-i-Cl**, being in the iron(II) proximity; (2) 4−12 ms for $\beta$-pyrrolic, 2,3-H of **2-o-Cl**, and *o*-aryl protons; (3) 25−40 ms for *m*-aryl protons; (4) 50−75 ms for *p*-phenyl groups; (5) above 100 ms for methoxyl groups. The above equation leads to a linear dependence between $T_1$ and $r$ in a bilogarithmic scale, with the slope equal to 6. Figure 4 shows the $T_1$ dependences on $r$ for both **2-o-Cl** and **2-i-Cl**. The $r$ values are obtained from MM+ models (Figure 5) and are averaged for protons equivalent in the $^1$H NMR spectrum. The fit is sufficiently accurate to confirm the proposed conformations.

Strikingly, the NMR features of the 2,3-H signal of **2-o-Cl** are similar to those of $\beta$-pyrrole resonances regarding the chemical shift (26 ppm), half-width (50 Hz), and relaxation time $T_1$ (8.6 ms, all for toluene-$d_8$, 298 K). For this "$\beta$-butadiene" position, the nitrogen donor atom seems to be unnecessary for the relaxation mechanisms operating (which is consistent with the presumed domination of the dipolar relaxation).

**Table 2. Relaxation Times $T_1$ for 2-Cl Measured by an Inversion−Recovery Technique**

| | $T_1$ (ms)[a] | |
|---|---|---|
| proton name | **2-o-Cl** | **2-i-Cl** |
| 1,4-H | 0.14 | 0.75 |
| 2,3-H | 8.6 | 0.17 |
| pyrrole 8,17 | 4.6 | 6.9 |
| pyrrole 7,18 | 11.9 | 4.8 |
| pyrrole 12,13 | 4.4 | 3.6 |
| *o*-Ph | $4 < T_1 < 7$ | 6.0 |
| *o*-Ar | 6.7; 6.7 | 6.5; 6.6 |
| *m*-Ph | ~25 | 27.5 |
| *m*-Ar | 31.0; $15 < T_1 < 60$ | 39.0; 37.6 |
| *p*-Ph | 75.1 | 52.1 |
| $OCH_3$ | 132.9 | 115.6 |

[a] All data for 298 K, toluene-$d_8$, 600 MHz.

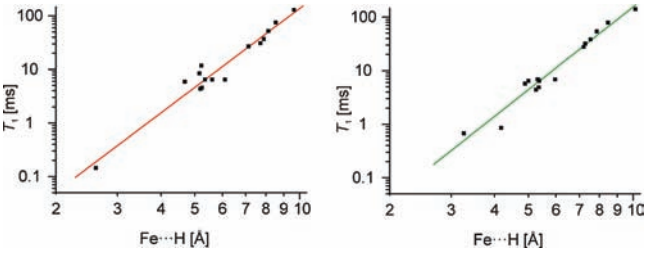


**Figure 4.** Dependencies $T_1$ on the Fe···H distance in logarythmic scales for **2-o-Cl** (left) and **2-i-Cl** (right).

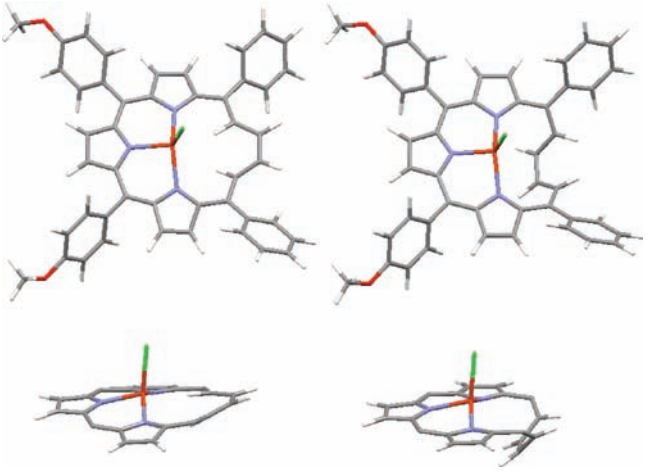

**Figure 5.** MM+ models of **2-o-Cl** and **2-i-Cl** (in side views, aryl groups omitted for clarity).

$T_1$ data analysis, together with 2D COSY and NOESY spectra, allowed assignment of all of the aryl signals (Figure 1C and Table 1). The 5,20-*meso*-phenyls of each form give one set of ortho−meta−para signals, proving the fast rotation of the rings. On the contrary, both ortho and meta protons of 10,15-*meso*-methoxyphenyls are differentiated (at 300 K), distinguishing between the "up" and "down" side of the macrocycle.


dx.doi.org/10.1021/ic2015176 |*Inorg. Chem.* 2011, 50, 10956–10965

The large negative chemical shifts of 1,4-protons of **2-o-X** (−163 to −220 ppm at 298 K, depending on the axial ligand) are without precedence for iron(II) porphyrins. Very large but positive isotropic shifts were recorded for the inner protons of the C−H groups of iron(II) carbaporphyrin complexes. For several complexes of carbaporphyrinoids, the rings with internal carbon atoms are sharply bent from a porphyrin plane, allowing side-on interaction of a central ion with the inner C−H fragment. The uniquely large positive isotropic shift of the inner hydrogen atom [over 1000 ppm, for an iron(II) inverted porphyrin] is a diagnostic sign of $Fe^{II}\cdots C-H$ agostic interaction.[34−37] The geometric relationship of iron(II) and C−H is, however, essentially different from that of **2-o-X**.

The paramagnetic shifts of **2-o-X** and **2-i-X** are generally in the range typical for high-spin iron(II) core-modified porphyrins, i.e., carbaporphyrins, heteroporphyrins, inverted, N-substituted porphyrins, and can be explained by a model typically applied to these compounds.[34−39] In the case of a high-spin iron(II) center, $(d_{xy})^2(d_{xz}d_{yz})^2(d_{z^2})^1(d_{x^2-y^2})^1$, both $\sigma$ and $\pi$ routes of spin-density delocalization can operate. The contact shift predominates for the resonances of protons in $\beta$ positions, yielding their downfield shifts. The typical delocalization pathways involve delocalization through a $\sigma$ framework by way of a $\sigma$ donation to the half-occupied iron(II) $d_{x^2-y^2}$ orbital. The differentiation of paramagnetic shifts for **2-X** is characteristic for the above-mentioned porphyrinoids and markedly larger than that in porphyrins of higher symmetry and may be accounted for by specific $\pi$-delocalization mechanisms discussed in detail for iron(III) porphyrins.[40,41]

**Conformational Rearrangements of 2-X.** The relative intensity of the signals of the **2-o-X** and **2-i-X** forms depends on an axial ligand, the solvent, and the temperature, but, in general, it is not simply a function of these parameters. The ratio varies to some extent from one synthesis to another and from one sample to another.

The controlled and reproducible conversion of form **in** to form **out** is achieved by heating a sample (a mixture of **out** and **in** isomers) in toluene, above 340 K. Up from this temperature, the ratio [**out**]:[**in**] is a function of the temperature and is determined by an anionic ligand. Thus, only at higher temperatures does isomerization occur at a reasonable rate and is thermodynamic equilibrium reached. The mechanism possibly involves axial ligand dissociation because axial ligand exchange also is observed only at higher temperatures (see below).

In an NMR experiment, a sample of **2-I** was dissolved in toluene-$d_8$ and $^1$H NMR spectra were measured in the temperature range of 200−370 K with parameters chosen to correctly record the intensities (D1 = 1−0.3 s and SW = 220 ppm). The ratio of [**2-o-I**]:[**2-i-I**] ($K$) was calculated from integration of nonoverlapping signals after a baseline correction. In the temperature range of 200−320 K, the molar ratio [**2-o-I**]:[**2-i-I**], equal for an exemplary sample to 0.95:1, was not affected by the temperature changes even in longer periods of time (24 h). Heating the solution to 340 K and above induced the ratio changes, and the relative concentration of the **out** form increased from $K$ = 0.95:1 to 1.15:1 at 340 K and finally to 1.30:1 at 370 K. Upon cooling of the solution, the ratio went back to 1.15:1 (at 340 K) and stopped there, suggesting that the conformational exchange was practically frozen at this temperature. In contrast to **2-I**, the preference for the **2-i-X** form at higher temperature has been observed for **2-Br** ($K$ = 0.9) and **2-Cl** ($K$ = 0.7, values at 360 K in toluene-$d_8$).

**Axial Ligand Exchange.** Another dynamic process was detected in a solution of the complex, that is, an axial ligand exchange, traced easily by $^1$H NMR spectroscopy. For **2-I** dissolved in chloroform-$d$ at elevated temperature (330 K), replacement of axial iodide with chloride, originating from the solvent, $CDCl_3$, was observed. The reaction proceeds for both **out** and **in** forms, although the latter reacts more rapidly. After 8 h at 330 K, 28% of **2-o-I** converted into **2-o-Cl** and 38% of **2-i-I** converted into **2-i-Cl**. The calculation was based on the assumption that the axial ligand exchange is much faster than **out** $\rightleftarrows$ **in** isomerization. In fact, during this experiment, the overall [**out**]:[**in**] ratio was practically constant (39% of isomer **in** before the reaction and 41% after 8 h). Moreover, at 330 K **out** $\rightleftarrows$ **in** transformation was not observed in toluene-$d_8$.

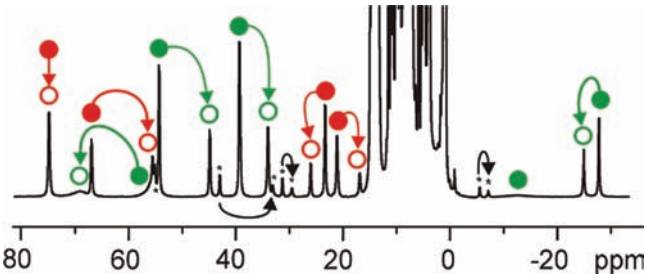


**Figure 6.** $^1$H NMR of **2-I** in chloroform-$d$ after 8 h at 330 K. Solid circles denote **2-I** and empty circles growing peaks of **2-Cl**. Isomer **out** is in red and **in** in green. Arrows represent EXSY peaks in the NOESY spectrum; impurities are marked by asterisks: **3-I** and **3-Cl**.

The NOESY spectrum measured at 330 K for the mixture of **2-I** and **2-Cl** in chloroform-$d$ showed EXSY cross-peaks (mixing times 0.01 and 0.02 s) between the respective signals of **2-o-I** and **2-o-Cl**, likewise **2-i-I** and **2-i-Cl** (Figure 6). The exchange correlations between forms **out** and **in** were not detected.

**Conformational Rearrangements of 2-$BF_4$.** The previously published[31,32] and aforementioned results indicate that flexibility seems to be an immanent quality of the vacataporphyrin ligand and that some tendencies are general for several metal ions. There are at least six possible reasonable conformational forms of metal(II) vacataporphyrin complexes,[32] and their relative energies (and energy barriers), depending on specific ions, may be calculated, whereas their physical accessibility has to be found for each case. That is to say, **in** and **out** forms were detected for most of the studied metals, i.e., cadmium(II), nickel(II), zinc(II), and, as shown above, iron(II). Their relative concentrations can be modulated by the temperature or light irradiation. Axial chloride subtraction from the palladium(II) vacataporphyrin complex resulted in profound conformational changes of the macrocycle, including the formation of an antiaromatic 18$\pi$-electron species with a Möbius strip delocalization pathway. Prompted by the latter studies, we have examined a similar reaction procedure for iron(II) complexes (expecting Möbius isomers or at least new isomers) to analyze the paramagnetic analogues. Consequently, the $^1$H NMR monitored titrations of **2-Cl**, **2-Br**, and **2-I** with a $AgBF_4$ solution were done, resulting in the identification of two new sets of peaks (Figure 7B), attributed to new forms of iron(II) vacataporphyrin. Their spectral patterns are independent from an axial halide in starting complexes.

The first set of signals (purple triangles in Figure 7B) is composed of five resonances of equal intensity, within the iron(II) vacataporphyrin chemical shift range, with differentiated half-widths. This set of signals, denoted as **2-*S*** (for *symmetric*), is attributed to a complex of 2-fold symmetry, with $BF_4^-$ as the counterion. The axial coordination of water was excluded because a reaction conducted in strictly water-free conditions

in a drybox did not suppress the formation of **2-*S***. The $T_1$ relaxation times of the five peaks are differentiated, falling, however, exactly in the range of **2-o-Cl** and **2-i-Cl** $T_1$ values. Three values (11.5, 9.6, and 7.5 ms) fit in the range observed for $\beta$-pyrrole or "$\beta$-annulene" protons, and the other two are much shorter but are not similar (1.4 and 0.2 ms), suggesting their proximity to the paramagnetic ion and attributed to 1,4-H and 2,3-H. Independently, an experiment with a specifically deuterated complex allowed assignment of the signal with $T_1$ = 1.4 ms to 1,4-H. Evidently, the $T_1$ values are similar to those of **2-i-Cl** with the 2,3-H proton closer to iron(II) than 1,4-H. Among possible iron(II) vacataporphyrin stereoisomers consistent with **2-*S*** spectral characteristics, one can construct at least three (**2-i**$^+$ corresponding to the **2-i-Cl** form and **2m**$^+$ and **2m**$'^+$ of Möbius topology) that match steric constraints imposed by $T_1$ data (Scheme 3). The dependence of $T_1$ vs $r$ (the Fe···H distances are estimated by appropriate MM+ models; see the Supporting Information) in logarithmic scales gives a fairly linear graph for each considered geometry, ruling out a definitive assignment of the structure based upon the available spectroscopic data.

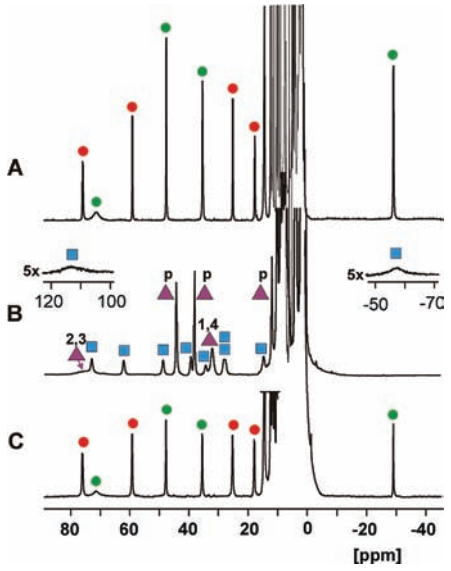


**Figure 7.** $^1$H NMR (600 MHz, toluene-$d_8$, 300 K) spectra: (A) **2-Br**; (B) [**2**$^+$][$BF_4^-$], **2-Br** after the addition of approximately 2 equiv of $AgBF_4$; (C) same solution after filtration under unaerobic conditions and $Et_4NBr$ (excess) addition. Annotations: p = pyrrole, red circle, **2-o-Br**; green circle, **2-i-Br**; blue square, **2-*A*-BF$_4$**; purple triangle, **2-*S*-BF$_4$**.

The second $^1$H NMR pattern, denoted as **2-*A*** (for *asymmetric*), consisting of 10 signals of equal intensity (blue squares, Figure 7B) is placed in a much wider window (+115 to −60 ppm) and provides evidence for full asymmetry of this form. The signal count is assigned to six pyrrole and four butadiene protons. Two signals at both borders of the spectrum are distinctly broader than others, suggesting the proximity of the respective protons to the paramagnetic center. The $T_1$ relaxation times of all 10 resonances are much shorter than those for all other forms (3 ms for three signals, ∼1 ms for seven signals, and below 1 ms for the two broadest signals). The asymmetric isomers (**2-a**$^+$, **2-a**$'^+$), which may explain the observed 10-peak NMR pattern, are shown in Scheme 4. The presence of two significantly broad butadiene resonances favors the structure **2-a**$^+$ with two protons (2,4-H) closer to the iron(II) center. There are two hypothetical structures with C2−Fe$^{II}$ $\sigma$-bond formation: with or without C2−H2 bond dissociation (structures **2-C** and **2-C′**, Scheme 4). The first possibility ($C_{sp^2}$-M) was observed for palladium vacataporphyrin complexes, but in the case of iron(II), the observation of 10 peaks excludes formation of **2C**. In any case of Fe−C $\sigma$-bond formation, the products of demetalation proceeded with deuterated acid, DCl (in $D_2O$), should give a free ligand selectively deuterated at C2. In fact, demetalation proceeded smoothly and quantitatively, but a monodeuterated product was never detected, excluding the $\sigma$-C coordination.

The ratio of new forms, [**2-*S***]:[**2-*A***], changes from one sample to another, but it is not dependent on the initial relative concentration of [**2-o-X**]:[**2-i-X**]. The formation of a **2-*S*/2-*A*** mixture from **2-o-X**/**2-i-X** is reversible because $Et_4NCl$ or $Et_4NBr$ addition to **2-*S*/2-*A*** (after removal of the solid byproduct, AgX)

**Scheme 3. Isomers of the Vacataporphyrin Complexes of 2-Fold Symmetry**

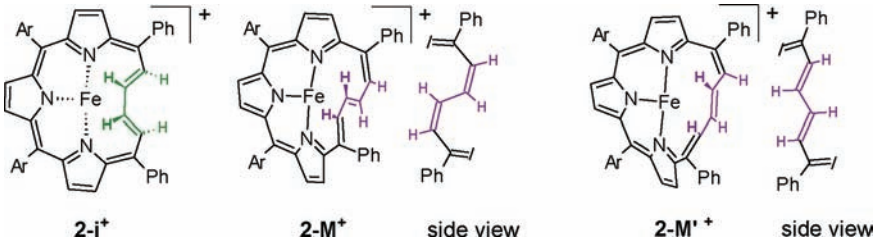


**Scheme 4. Asymmetric Isomers of the Iron(II) Vacataporphyrin Complexes**

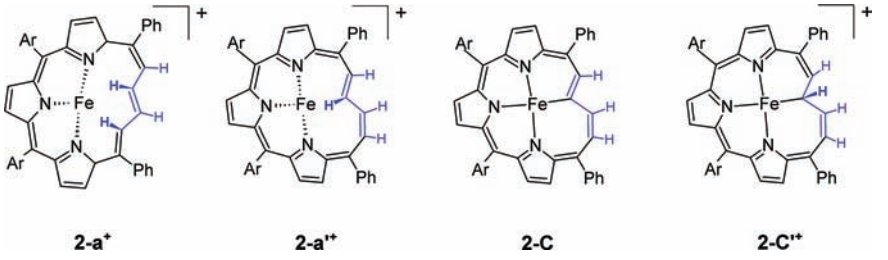



dx.doi.org/10.1021/ic2015176 |*Inorg. Chem.* 2011, 50, 10956–10965

recovers **2-o-X**/**2-i-X** but in a ratio different from the initial one. Methanol-$d_4$ addition transforms the **2-*S***/**2-*A*** mixture into a five-coordinate **2-o**-$(MeOD)^{2+}$ complex (see below).

A solution of **2-*S***/**2-*A*** is not stable in air or at higher temperature. Its oxidation with dry dioxygen gives an iron(II) 21-oxaporphyrin complex (identified after $Et_4NCl$ addition) and free ligand **1** (see below).

**Five-Coordinate Iron(II) Vacataporphyrin Complexes.** The addition of an excess of methanol-$d_4$ (50% v/v) to a toluene sample of **2** being a mixture of isomers, **out**/**in** or ***S***/***A***, converts the initial forms into a single five-coordinate bis(alcohol) cationic complex $[\mathbf{2}\text{-}(MeOD)_2]^+$. The $^1$H NMR spectrum of the **2-o-Cl**/**2-i-Cl** sample (toluene-$d_8$) measured immediately (about 3 min) after methanol-$d_4$ addition showed the presence of a small percentage of the **in** form, but after 15 min, the only form present in the solution was $[\mathbf{2}\text{-o}\text{-}(MeOD)_2]^+$ (Figure 8B). As expected, an excess of the solvent acting as a ligand and saturating the axial positions favors the form **out**, where the butadiene moiety does not block the second axial coordinating site of the iron ion. The **out** conformation of the annulenic part of the vacataporphyrin ligand is preserved when the solvents are evaporated to dryness, and the remaining solid is dissolved in toluene-$d_8$. The original axial ligand (chloride) replaced methanol, and identical chemical shifts were registered like for the original toluene solution of **2-o-Cl** (excluding any axial ligand exchange) and almost pure isomer **out** was obtained (Figure 8C and Scheme 5).

To study in detail the axial ligand exchange and formation of five-coordinate complexes, $^1$H NMR titration of **2-I** was done for an exemplary nitrogen ligand: imidazole. In the course of titration, a difference in the reactivity of the isomers toward the nitrogen ligand became evident. The first portions of imidazole reacted with **2-o-I** and the signals of **2-o** slightly moved, while the signals of **2-i-I** were not disturbed. This may be interpreted as the formation of five-coordinate **2-o-I**-Im with two different axial ligands, which remains in fast equilibrium with **2-o-I**. After the addition of 0.7 equiv of imidazole, new signals appeared, attributed to $[\mathbf{2}\text{-o}\text{-}Im_2]^+$, which grow at the expense of signals of a **2-o-I**-Im $\rightleftarrows$ **2-o-I** mixture and, after these are almost consumed, at the expense of **2-i-I**.

The NMR pattern of $[\mathbf{2}\text{-o}\text{-}Im_2]^+$ signals, with four vacataporphyrin signals shifted downfield in the range 70−25 ppm, is similar to that of the bis(alcohol) complex attributed to the **out** form. For $[\mathbf{2}\text{-o}\text{-}Im_2]^+$, the 1,4-H resonance strongly upfield shifted was detected at −118.3 ppm. Paramagnetically shifted protons of coordinated imidazole were easily assigned by the reaction with $D_2O$ (N1−H was exchanged to N1−D) and with specifically deuterated imidazole (imidazole-*1,2-*$d_2$). The 4-H imidazole signal has not been detected probably because of its large width. The relative intensity of the imidazole and porphyrin signals is consistent with the above bis(imidazole) complex stoichiometry.

**Oxygenation of 2-o-X to Iron(II) 21-Oxaporphyrin.** The $^1$H NMR samples (toluene-$d_8$) of **2-X** prepared in dry and oxygen-free atmospheres of a glovebox are stable for weeks at the low temperature of a freezer (about −18 °C). When the solution is exposed to dry dioxygen at 300 K, **2-o-X** undergoes slowly (hours) an unprecedented oxygenation, yielding the iron(II) 21-oxaporphyrin complex characterized previously in detail by $^1$H NMR[38] **3-X** (Scheme 6). Regarding solely the porphyrin's building blocks, a butadiene unit is oxidized to a furan ring without a change of the porphyrin perimeter. In fact, the reaction is, in some sense, reverse to the synthesis of vacataporphyrin, achieved by extrusion of tellurium from 21-telluraporphyrin.[28]

The $^1$H NMR experiment following the reaction of **2-I** with dioxygen is presented in Figure 9. As demonstrated by a characteristic spectroscopic pattern (blue dots, Figure 9 B), the iron(II) oxidation state has been conserved in the course of the

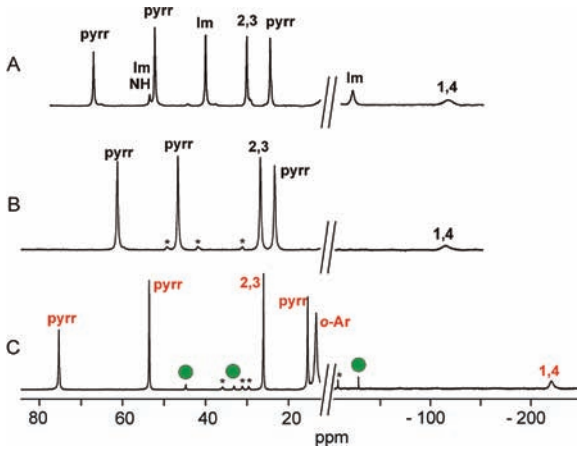


**Figure 8.** $^1$H NMR spectra (300 K) of (A) $[\mathbf{2}\text{-o}\text{-}(Im)_2]^+$ in toluene-$d_8$, imidazole partially deuterated at NH, (B) $[\mathbf{2}\text{-o}\text{-}(MeOD)_2]^+$ in methanol-$d_4$/toluene-$d_8$ (1:1, v/v), and (C) **2-o-Cl** in toluene-$d_8$. Traces of **2-i-Cl** are marked by green circles; impurity **3-Cl** is marked by asterisks.

**Scheme 6. Oxygenation of 2-o-X**

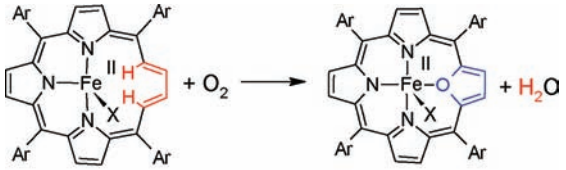


**Scheme 5. Formation of Five-Coordinate Vacataporphyrin Complexes**

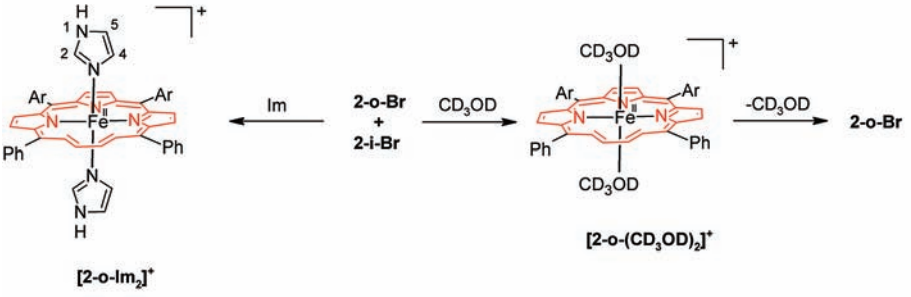



dx.doi.org/10.1021/ic2015176 |*Inorg. Chem.* 2011, 50, 10956–10965

macrocyclic transformation. The resulting iron(II) 21-oxaporphyrin is known to stabilize low oxidation states of iron, and **3-X** is air-stable. While **2-o-I** is gradually consumed in the reaction, **2-i-I** remains unchanged (Figure 9B) provided that the reaction is carried out at temperatures below 330 K to prevent any **out** ⇄ **in** isomerization. After 8 h (at 300 K), the solution contains only **2-i-I** and **3-I** (Figure 9C). Heating this sample for a few minutes at 370 K restored the equilibrium concentration of **2-i-I** (Figure 9D).

Integration of the signals of **2-o-I**, **2-i-I** (used here as an intensity standard), and **3-I** through the experiment shows a significant difference between the ratio [**2-o-I**]:[**2-i-I**] in the initial sample and the ratio [**3-I**]:[**2-i-I**] in the final solution and indicates that the yield of the **2-o-I** → **3-I** transformation is far from quantitative. The important side products are the free ligand **1** and $\mu$-oxo dimer of iron(III) oxaporphyrin **4** (Chart 3),[38] marked by * and # in Figure 9C.

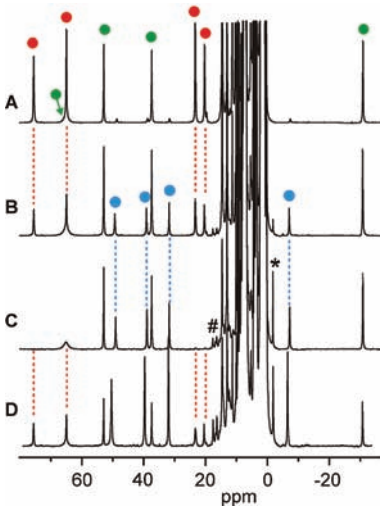


**Figure 9.** $^1$H NMR spectra (600 MHz, 300 K, toluene-$d_8$) of (A) **2-I**, (B) the sample after 3 h in a dry oxygen atomosphere (**3-I** is marked with blue dots), (C) the sample after 8 h (*, the NH signal of **1**; #, signals of $\mu$-oxo dimer **4**); (D) the sample from part C after 5 min in 370 K. Labeling: red dots, **2-o-I**; green dots, **2-i-I**; blue dots, **3-I**.

**Chart 3. Iron(III) Oxaporphyrin $\mu$-Oxo Dimer**

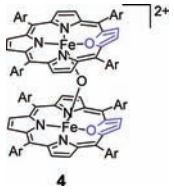


**4**

Attempts to trap any intermediates at low temperature (200−240 K) were unsuccessful because the reaction is relatively slow and the intermediates must have very low concentrations. A facile formation of **4** (which is not formed from **3-X** just under $O_2$) gives, however, some suggestions of possible intermediates, preorganized to form $\mu$-oxo dimer **4**. One of the conceivable mechanisms of the transformation of **2-o-X** to **3-X** is presented in Scheme 7. The first step, activating the inert $O_2$ molecule, is probably its binding to the iron(II) ion, sterically possible only for the **2-o-X** isomer with one side of the macrocycle plane available for oxygen attack. In the more inert **2-i-X** form, one side of the complex is blocked by an axial halide X and the opposite by the bent butadiene chain. The second step, the formation of a −O−O− bridge between iron(II) and C2, is relevant to a mechanism proposed for the conversion of verdoheme to biliverdin.[42] The following processes are −O−O− cleavage and intramolecular oxidation. The activated C−H bonds are C1−H1 and C4−H4, the closest to the bound oxygen molecule for the **out** conformation.

The reaction mixture after demetalation with concentrated hydrochloric acid (stirring for 30 min at room temperature), was searched for other oxidation products, like 2-hydroxy- or 2-oxovacataporphyrin, but none was detected by $^1$H NMR or mass spectrometry. In fact, the products of demetalation were neutralized with triethylamine and identified as a surprisingly clean mixture of vacataporphyrin free base and 21-oxaporphyrin.

**Conclusions.** An annulene−porphyrin hybrid, vacataporphyrin, is a porphyrin devoid of one nitrogen or, in other words, having a four-carbon chain in the macrocyclic perimeter in place of one pyrrole ring. It acts as a versatile ligand, binding a variety of transition-metal ions. Here the high-spin iron(II) center allowed us to study the conformational changes of the vacataporphyrin perimeter by means of relaxation time ($T_1$) studies and $^1$H NMR paramagnetic shifts. The results gave us another argument that the flexibility of the annulene fragment is an immanent quality of vacataporphyrin and may be controlled by the axial ligand addition or subtraction and temperature.

Originally, two isomers have been detected for the vacataporphyrin iron(II) complex with one axial halide anion, differing in the configuration of the annulene fragment, which acquires

**Scheme 7. Proposed Mechanism of 2-o-X Oxidation**[a]

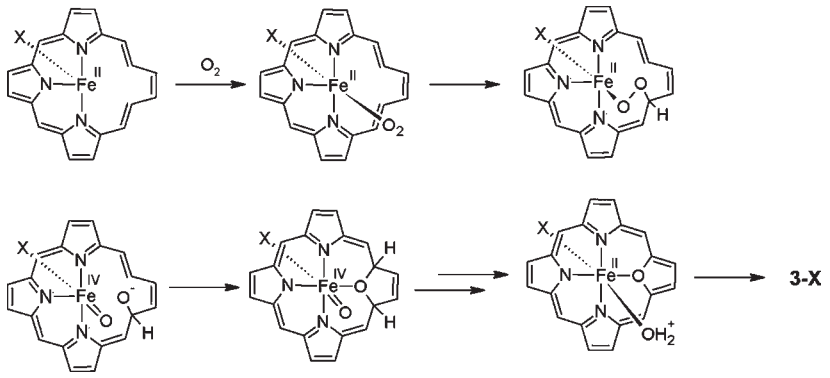


[a] Aryl substituents are not presented for clarity.


dx.doi.org/10.1021/ic2015176 |*Inorg. Chem.* 2011, 50, 10956–10965

planar (isomer **out**) or bent (isomer **in**) geometry. On the other hand, axial halide subtraction allowed us to observe two more isomeric forms of iron(II) vacataporphyrin with a $BF_4^-$ counterion differentiated by conformation of the butadiene linker. Moreover, there is a significant difference in the reactivity of the isomers, connected with the different accessibilities of the iron center for a reagent. Solely, the isomer **out** reacts with dioxygen, which leads iron(II) 21-oxaporphyrin. The mechanism of the reaction involves the peculiar incorporation of an oxygen atom in the butadiene fragment to form a furan ring. The intramolecular reactivity toward dioxygen bears some importance for the initial stages of verdoheme clevage in the course of coupled oxidation of heme.

## EXPERIMENTAL SECTION

**Solvents and Reagents.** Chloroform-*d* was passed through basic $Al_2O_3$. All of the NMR solvents (toluene, toluene-$d_8$, chloroform-*d*, and methanol-$d_4$) were deoxygenated by a freeze−pump−thaw technique. THF was distilled under dinitrogen over sodium/benzophenone. Imidazole-*1,2*-$d_2$ was prepared according to the reported method.[43]

Vacataporphyrin [5,20-diphenyl-10,15-bis(4-metoxyphenyl)-21-vacataporphyrin] has been obtained according to the previously described procedures.[31] The deuterated ligand **1**-$d_x$ was synthesized as published before,[31] and the degree of deuteration ($x$) varied much depending on the reaction conditions, mainly the reaction time (Table S2 in the Supporting Information). The reaction time was optimized to maximize the yield for two available DCl concentrations: a higher concentration of DCl (35% in $D_2O$) required shorter reaction time (50−60 min) and yielded a ligand with a generally lower degree of deuteration. A higher deuterium substitution level was obtained for longer reaction time, 1 h 30 min, applied for 20% DCl.

**2-Cl**: Vacataporphyrin **1**[28,31] (13 mg, 0.020 mmol) was dissolved in freshly distilled THF (15 mL), and nitrogen was bubbled through the solution for 20 min. $FeCl_2 \cdot 4H_2O$ (11 mg, 0.057 mmol) was added, and the solution was refluxed under nitrogen for about 20 min. The color changed from peach-red to bright green, and the solvent was distilled off, still under nitrogen. The flask with the dry residue was immediately introduced to the glovebox, and $^1$H NMR samples were prepared by extracting the solid with toluene-$d_8$ and filtering the suspension through glass wool directly to an NMR tube.

$^1$H NMR for **2-o-Cl** (500 MHz, toluene-$d_8$, 298 K): $\delta$ 75.2 (2H, pyrr 12,13), 53.4 (2H, pyrr 7,18), 26.0 (2H, vac 2,3), 15.4 (2H, pyrr 8,17), 13.3 (4H, *o*-Ph), 10.9 (4H, *m*-Ph), 10.7 (2H, *m*-Ar), 9.4 (2H, *p*-Ph), 4.1 (6H, $OCH_3$), 3.4 (2H, *m*-Ar), −0.2 (2H, *o*-Ar), −2.5 (2H, *o*-Ar), −220.2 (2H, vac 1,4). $^1$H NMR for **2-i-Cl** (500 MHz, toluene-$d_8$, 298 K): $\delta$ 75.2 (2H, vac 2,3), 44.7 (2H, pyrr 8,17), 33.1 (2H, pyrr 12,13), 13.8 (2H, *o*-Ar), 11.0 (4H, *o*-Ph), 9.6 (2H, *p*-Ph), 8.8 (4H, *m*-Ph), 8.2 (2H, *m*-Ar), 4.9 (2H, *m*-Ar), 3.4 (6H, $OCH_3$), 2.8 (2H, *o*-Ar); −28.4 (2H, pyrr 7,18). HRMS (ESI). Calcd for $[M - Cl]^+$ ($C_{46}H_{36}N_3O_2{}^{55}Fe^+$): $m/z$ 716.2011. Found: $m/z$ 716.1992. UV−vis [toluene; $\lambda_{max}$, nm (log $\varepsilon$)]: 443 (4.4), 550 (3.3), 617 (sh), 651 (3.6), 711 (3.5);

**2-Br** was synthesized in the same manner using $FeBr_2$ instead of $FeCl_2 \cdot 4H_2O$. $^1$H NMR for **2-o-Br** (500 MHz, toluene-$d_8$, 298 K): $\delta$ 76.0 (2H, pyrr 12,13), 59.0 (2H, pyrr 7,18), 25.0 (2H, vac 2,3), 17.5 (2H, pyrr 8,17), −193.0 (2H, vac 1,4). $^1$H NMR for **2-i-Br** (500 MHz, toluene-$d_8$, 298 K): $\delta$ 71.7 (2H, vac 2,3), 47.5 (2H, pyrr 8,17), 35.1 (2H, pyrr 12,13), −30.0 (2H, pyrr 7,18). HRMS (ESI). Calcd for $[M - Br]^+$ ($C_{46}H_{36}N_3O_2{}^{55}Fe^+$): $m/z$ 716.1999. Found: $m/z$ 716.1992. UV−vis (toluene, $\lambda_{max}$, nm): 443 (4.4), 617 (sh), 655 (3.7), 714 (3.8).

**2-I**. Vacataporphyrin **1** (25 mg; 0.038 mmol) was dissolved in freshly distilled THF (15 mL), and nitrogen was bubbled through the solution for 20 min. $Fe(CO)_5$ (37 mg, 0.19 mmol) and $I_2$ (10 mg, 0.079 mmol)[44] were added, and the solution was refluxed under nitrogen for about 20 min. The solvent was distilled off, still under nitrogen. The flask with the dry residue was immediately introduced to the glovebox, and $^1$H NMR samples were prepared by extracting the solid with toluene-$d_8$ or $CDCl_3$ and filtering the suspension through glass wool directly to an NMR tube.

$^1$H NMR for **2-o-I** (500 MHz, toluene-$d_8$, 298 K): $\delta$ 75.2 (2H, pyrr 12,13), 64.5 (2H, pyrr 7,18), 23.1 (2H, vac 2,3), 20.3 (2H, pyrr 8,17), −162.5 (2H, vac 1,4). $^1$H NMR for **2-i-I** (500 MHz, toluene-$d_8$, 298 K): $\delta$ 64.5 (2H, vac 2,3), 52.7 (2H, pyrr 8,17), 37.2 (2H, pyrr 12,13), −30.9 (2H, pyrr 7,18). HRMS (ESI). Calcd for $[M - I]^+$ ($C_{46}H_{36}N_3O_2{}^{55}Fe^+$): $m/z$ 716.1999. Found: $m/z$ 716.1992. UV−vis (toluene; $\lambda_{max}$, nm): 443 (4.4), 617 (sh), 657 (3.7), 714 (3.6).

**2-BF$_4$**. A sample of **2-Cl** (or **2-Br** or **2-I**) in an NMR tube was titrated with a saturated toluene-$d_8$ solution of $AgBF_4$ under NMR control at 300 K. When the formation of **2-BF$_4$** was complete according to $^1$H NMR, the sample was transferred to a glovebox, AgX was filtered off, and the clear sample was used for further studies.

$^1$H NMR for **2-*A*-BF$_4$** (600 MHz, toluene-$d_8$, 300 K): $\delta$ 113.1, 72.9, 62.1, 48.6, 39.0, 34.5, 28.0, 14.3, −55.1. $^1$H NMR for **2-*S*-BF$_4$** (600 MHz, toluene-$d_8$, 300 K): $\delta$ 76.4 (1H, 2,3-H), 44.4 (1H, pyrr), 38.1 (1H, pyrr), 32.9 (1H, 1,4-H), 11.9 (1H, pyrr).

**MM+ Models.** In the minimization procedure, we have used the standard MM+ parametrization of the *HyperChem* program with the exception of the iron coordination surroundings, where we have imposed the constraints reflecting the high-spin state of the iron(II) ion applying the respective data determined previously for iron(II) 21-thiaporphyrin.[19]

**Instrumentation.** NMR spectra were recorded on Bruker Avance 500 MHz and Bruker Avance III 600 MHz spectrometers. UV−vis electronic spectra were recorded on a Varian Cary 50 Bio spectrometer. Mass spectra were recorded on a Bruker micrOTOF-Q spectrometer using the electrospray ionization (ESI) technique.

## ASSOCIATED CONTENT

**Supporting Information.** Dependencies $T_1$ on the Fe···H distance in logarythmic scales, $^1$H NMR chemical shifts, and percentage of deuteration of different sites of ligand **1**. This material is available free of charge via the Internet at http://pubs.acs.org.

## AUTHOR INFORMATION

### Corresponding Author

*E-mail: lechoslaw.latos-grazynski@chem.uni.wroc.pl (L.L.-G.), ewa.dudziak@chem.uni.wroc.pl (E.P.-D.). Tel: +48 71 3757256. Fax: +48 71 3282348. Homepage: http://llg.chem.uni.wroc.pl/.

## ACKNOWLEDGMENT

Financial support from the Ministry of Science and Higher Education (Grant N204 013536) is kindly acknowledged.

## REFERENCES

(1) Bertini, I.; Luchinat, C.; Parigi, G.; Pierattelli, R. *Dalton Trans.* **2008**, 3782–3790.
(2) Rivera, M.; Zeng, Y. *J. Inorg. Biochem.* **2005**, *99*, 337–354.
(3) Turano, P. Heme Acquisition by Hemophores: A lesson from NMR. In *Handbook of Porphyrin Science*; Kadish, K. M., Smith, K. M., Guilard, R., Eds.; World Scientific: Singapore: 2010; pp 339−365.
(4) Bertini, I.; Turano, P.; Vila, A. J. *Chem. Rev.* **1993**, *93*, 2833–2932.
(5) Bertini, I.; Luchinat, C. *Coord. Chem. Rev.* **1996**, *150*, 29–75.

(6) Goff, H. M. Nuclear Magnetic Resonance of Iron Porphyrins. In *Iron Porphyrins*; Lever, A., Ed.; Addison-Wesley: Reading, MA, 1983; pp 237−281.
(7) Walker, F. A. Proton NMR and EPR Spectroscopy of Paramagnetic Metalloporphyrins. In *The Porphyrin Handbook*; Kadish, K. M., Smith, K. M., Guilard, R., Eds.; Academic Press: San Diego, CA, 2000; pp 81−183.
(8) Walker, F. A. *Chem. Rev.* **2004**, *104*, 589–616.
(9) Nakamura, M.; Ohgo, Y.; Ikezaki, A. Electronic and Magnetic Structures of Iron Porphyrin Complexes. In *Handbook of Porphyrin Science*; Kadish, K. M., Smith, K. M., Guilard, R., Eds.; World Scientific: Singapore, 2010; pp 1−146.
(10) Walker, F. A. NMR and EPR Spectroscopy of Paramagnetic Metalloporphyrins and Heme Proteins. In *Handbook of Porphyrin Science*; Kadish, K. M., Smith, K. M., Guilard, R., Eds.; World Scientific: Singapore, 2010; pp 1−337.
(11) Nakamura, M. *Coord. Chem. Rev.* **2006**, *250*, 2271–2294.
(12) Ohgo, Y.; Hoshino, A.; Okamura, T.; Uekusa, H.; Hashizume, E.; Ikezaki, A.; Nakamura, M. *Inorg. Chem.* **2007**, *46*, 8193–8207.
(13) Jentzen, W.; Ma, J.-G.; Shelnutt, J. A. *Biophys. J.* **1998**, *74*, 753–763.
(14) Ma, J.-G.; Zhang, J.; Franco, R.; Jia, S.-L.; Moura, I.; Moura, J. J. G.; Kroneck, P. M. H.; Shelnutt, J. A. *Biochemistry* **1998**, *37*, 12431–12442.
(15) Shelnutt, J. A.; Song, X.-Z.; Ma, J.-G.; Jia, S.-L.; Jentzen, W.; Medforth, C. J. *Chem. Soc. Rev.* **1998**, *27*, 31–41.
(16) Ma, J.-G.; Leberge, M.; Song, X.-Z.; Jentzen, W.; Jia, S.-L.; Zhang, J.; Vanderkooi, J. M.; Shelnutt, J. A. *Biochemistry* **1998**, *37*, 5118–5128.
(17) Senge, M. O. Highly Substituted Porphyrins. *The Porphyrin Handbook*; Academic Press: San Diego, CA, 2000; p 239.
(18) Latos-Grażyński, L.; Lisowski, J.; Olmstead, M. M.; Balch, A. L. *J. Am. Chem. Soc.* **1987**, *109*, 4428–4429.
(19) Latos-Grażyński, L.; Lisowski, J.; Olmstead, M. M.; Balch, A. L. *Inorg. Chem.* **1989**, *28*, 1183–1188.
(20) Hung, C.-H.; Ou, C.-K.; Lee, G.-H.; Peng, S.-M. *Inorg. Chem.* **2001**, *40*, 6845–6847.
(21) Pawlicki, M.; Latos-Grażyński, L. Carbaporphyrinoids—Synthesis and Coordination Properties 203. In *Handbook of Porphyrin Science: with Applications to Chemistry, Physics, Materials Science, Engineering, Biology and Medicine*; Kalish, H., Smith, K. M., Guilard, R., Eds.; World Scientific Publishing: Singapore, 2010; pp 104−192.
(22) Chmielewski, P. J.; Latos-Grażyński, L. *Coord. Chem. Rev.* **2005**, *249*, 2510–2533.
(23) Stępień, M.; Latos-Grażyński, L. *Acc. Chem. Res.* **2005**, *8*, 88–98.
(24) Pacholska, E.; Latos-Grażyński, L.; Ciunik, Z. *Angew. Chem., Int. Ed.* **2001**, *40*, 4466–4469.
(25) Stępień, M.; Latos-Grażyński, L. *J. Am. Chem. Soc.* **2002**, *124*, 3838–3839.
(26) Stępień, M.; Latos-Grażyński, L.; Szterenberg, L. *Inorg. Chem.* **2004**, *43*, 6654–6662.
(27) Szyszko, B.; Latos-Grażyński, L. *Organometallics* **2011**, *30*, 4354–4363.
(28) Pacholska, E.; Latos-Grażyński, L.; Ciunik, Z. *Chem.—Eur. J.* **2002**, *8*, 5403–5406.
(29) Lash, T. D.; Jones, S. A.; Ferrence, G. M. *J. Am. Chem. Soc.* **2010**, *132*, 12786–12787.
(30) Pacholska-Dudziak, E.; Szterenberg, L.; Latos-Grażyński, L. *Chem.—Eur. J.* **2011**, *17*, 3500–3511.
(31) Pacholska-Dudziak, E.; Skonieczny, J.; Pawlicki, M.; Latos-Grażyński, L.; Szterenberg, L. *Inorg. Chem.* **2005**, *44*, 8794.
(32) Pacholska-Dudziak, E.; Skonieczny, J.; Pawlicki, M.; Szterenberg, L.; Ciunik, Z.; Latos-Grażyński, L. *J. Am. Chem. Soc.* **2008**, *130*, 6182–6195.
(33) Pacholska-Dudziak, E.; Latos-Grażyński, L. *Coord. Chem. Rev.* **2009**, *253*, 236–248.
(34) Rachlewicz, K.; Wang, S.-L.; Peng, C.-H.; Hung, C.-H.; Latos-Grażyński, L. *Inorg. Chem.* **2003**, *42*, 7348–7350.
(35) Rachlewicz, K.; Gorzelańczyk, D.; Latos-Grażyński, L. *Inorg. Chem.* **2006**, *45*, 9742.
(36) Myśliborski, R.; Rachlewicz, K.; Latos-Grażyński, L. *Inorg. Chem.* **2006**, *45*, 7828–7834.
(37) Hung, C.-H.; Chang, F.-C.; Lin, C.-Y.; Rachlewicz, K.; Stępień, M.; Latos-Grażyński, L.; Lee, G.-H.; Peng, S.-M. *Inorg. Chem.* **2004**, *43*, 4118–4120.
(38) Pawlicki, M.; Latos-Grażyński, L. *Inorg. Chem.* **2002**, *41*, 5866.
(39) Balch, A. L.; Chan, Y.-W.; La Mar, G. N.; Latos-Grażyński, L.; Renner, M. W. *Inorg. Chem.* **1985**, *24*, 1437.
(40) Cheng, R.-J.; Chen, P.-Y.; Lovell, T.; Liu, T.; Noodleman, L.; Case, D. A. *J. Am. Chem. Soc.* **2003**, *125*, 6774–6783.
(41) Wojaczyński, J.; Latos-Grażyński, L.; Hrycyk, W.; Pacholska, E.; Rachlewicz, K.; Szterenberg, L. *Inorg. Chem.* **1996**, *35*, 6861–6872.
(42) Ortiz de Montellano, P. R. *Acc. Chem. Res.* **1998**, *31*, 543–549.
(43) Vaugh, J. D.; Mugharbi, Z.; Wu, E. C. *J. Org. Chem.* **1970**, *35*, 1141–1145.
(44) Rachlewicz, K.; Latos-Grażyński, L.; Vogel, E. *Inorg. Chem.* **2000**, *39*, 3247.